Pergamon

Int. J. Heat Mass Transfer. Vol. 38, No. 1, pp. 55–64, 1995

0017-9310/95 $9.50+0.00

0017-9310(94)00141-3

Computation of high-temperature near-wall heat transfer using an enthalpy balancing scheme

P. J. STUTTAFORD, S. ANGHAIE† and W. SHYY‡

Innovative Nuclear Space Power and Propulsion Institute, Department of Nuclear Engineering Sciences, 202 Nuclear Sciences Center, University of Florida, Gainesville, FL 32611-2055, U.S.A.

(*Received* 17 *November* 1993 *and in final form* 10 *May* 1994)

Abstract—The objective of this work is to analyze high-temperature, high heat-flux hydrogen flows under a variety of boundary conditions, in particular wall-heat flux boundary conditions. Both laminar and turbulent flows are investigated. An enthalpy balancing scheme is formulated and implemented allowing accurate, fast converging solutions of turbulent flows with high wall-heat flux boundary conditions. The solutions obtained are assessed along with several correlations proposed in the literature.

1. INTRODUCTION

Accurate calculation of near-wall heat transfer is of great importance to the design and operation of high-temperature high heat-flux systems. Nuclear thermal rocket propulsion is a case in point and is the driving force behind this investigation. The nuclear thermal rocket is the next generation of propulsion system for deep space missions. In a nuclear rocket, the hydrogen propellant flows through the reactor core and becomes heated to temperatures approaching 3000 K. A good understanding of the heat-transfer mechanism for such flow devices is critical for their successful operation.

Extensive work has been done in the field of laminar and turbulent-flow heat transfer in pipes. However, most of this work has been performed for cases in which conditions such as temperature and heat flux are not extreme. These studies were also normally confined to cases in which adiabatic and isothermal wall boundary conditions were used. The purpose of this study is to examine laminar and turbulent high-temperature, high heat-flux flows of hydrogen in a tube. Constant and variable wall-heat flux boundary conditions are specified in the analysis, as well as adiabatic and isothermal wall-boundary conditions. It is also intended to compare numerical results with the Nusselt number, calculated by using a number of common mechanistic correlations. The primary emphasis of this comparative evaluation effort is on the entrance effect and also on the use of real gas properties. If the gas properties vary significantly with the temperature, careful attention needs to be paid to the treatment of real gas properties at high near-wall temperature gradients.

It is generally known that, when computing fluid-flow and heat-transfer problems, normal gradient boundary conditions may result in slow convergence. A method of enthalpy balancing is developed and implemented which vastly improves the convergence rate when specifying wall-heat flux boundary conditions. This is similar in principal to mass rebalancing where mass conservation at the outflow boundary is enforced. Mass rebalancing has been successfully implemented in a number of numerical schemes. A comprehensive discussion of this method can be found in ref. [1].

2. FORMULATION OF THE NUMERICAL ALGORITHM

The present algorithm solves the thin-layer Navier–Stokes equations in which viscous effects are confined to thin-layer regions near the body surfaces. Viscous and heat conduction terms are represented by derivatives normal to the surface only. Streamwise viscous derivative terms and heat conduction are much smaller in magnitude, and can therefore be neglected.

The Navier–Stokes equations may be written in two-dimensional conservation form as

$$\frac{\partial \bar{U}}{\partial t}+\frac{\partial \bar{F}_i}{\partial z}+\frac{\partial \bar{G}_i}{\partial r}+\bar{H}_i=\frac{\partial \bar{G}_v}{\partial r}+\bar{H}_v \tag{1}$$

where

$$\bar{U}=\begin{bmatrix}\rho\\ \rho u\\ \rho v\\ e\end{bmatrix}\quad \bar{F}_i=\begin{bmatrix}\rho u\\ \rho u^2+p\\ \rho uv\\ (e+p)u\end{bmatrix}\quad \bar{G}_i=\begin{bmatrix}\rho v\\ \rho uv\\ \rho v^2+p\\ (e+p)v\end{bmatrix}$$

$$\bar{H}_i=\begin{bmatrix}\rho v\\ \rho uv\\ \rho v^2\\ (e+p)v\end{bmatrix} \tag{2}$$

†Author to whom correspondence should be addressed.

‡Department of Aerospace Engineering, Mechanics and Engineering Science.

NOMENCLATURE

c_p	specific heat at constant pressure
c_v	specific heat at constant volume
d	diameter
e	total energy per unit volume
h	heat transfer coefficient
i_{max}	total number of axial grid points
j_{max}	total number of radial grid points
k	thermal conductivity, or turbulence model constant
l	pipe length
M	mass flow rate
Nu	Nusselt number, hd/k
p	pressure
Pr	Prandtl number, $c_p\mu/k$
q_c	conductive heat flux
q_w	wall heat flux
Q	total heat flux
r	radial position measured from the centerline
R	pipe radius
Re	Reynolds number, ul/v
t	time
T	temperature
u	axial velocity, z-component
v	radial velocity, r-component
y	radial position measured from the wall
z	axial position measured from the pipe entrance.

Greek symbols

ε	heat balance correction factor
μ	dynamic viscosity
ρ	density
ω	heat balance relaxation factor
$\lvert\omega\rvert$	magnitude of vorticity.

Subscripts

1	inside wall boundary mesh point
2	inside fluid boundary mesh point
b	bulk conditions
i	axial mesh point locations
j	radial mesh point locations
t	turbulent component
w	wall conditions.

and the viscous terms are

$$\bar{G}_v = \begin{bmatrix} 0 \\ \mu_T \overline{\frac{\partial u}{\partial r}} \\ 4\frac{\mu_T}{3}\frac{\partial v}{\partial r} - \frac{2}{3}\mu_T\frac{v}{r} \\ \mu_T u\frac{\partial u}{\partial r} + 4\frac{\mu_T}{3}v\frac{\partial v}{\partial r} q_c \end{bmatrix} \tag{3}$$

$$\bar{H}_v = \frac{1}{r}\begin{bmatrix} 0 \\ \mu_T \overline{\frac{\partial u}{\partial r}} \\ 2\mu_T\left(\frac{\partial v}{\partial r} - \frac{v}{r}\right) \\ \mu_T u\frac{\partial u}{\partial r} + \frac{4}{3}\mu_T v\frac{\partial v}{\partial r} - q_c \end{bmatrix}. \tag{4}$$

In the above formulation, ρ represents density, u and v are the velocity components in the z (axial) and r (radial) directions, respectively, q_c is the conductive heat flux, p is the pressure, e represents the total energy per unit volume, and μ_T represents the total viscosity, i.e. molecular, μ_l, and eddy, μ_t, components.

The algorithm used is based on MacCormack's predictor/corrector scheme. It is a hybrid explicit/implicit method [2], employing a finite volume approach. Unlike the finite difference approach where mesh points are placed directly on the boundaries, the finite volume approach places volume–cell surfaces along the boundaries with the mesh points located at the cell centers a half-mesh spacing away. The finite volume formulation computes fluxes crossing the cell surfaces. This approach makes the implicit coefficient matrices more diagonally dominant, and thus easier to solve. This is an important factor when using line Gauss–Seidel iteration to obtain a solution, as is the case here. Alternating the sweeping in the backward and forward streamwise directions improves the solution convergence. The hybrid implicit/explicit algorithm may be summarized as follows:

Predictor

$$\Delta U^n_{i,j} = -\Delta t\left[\frac{D_+ \cdot F_i}{\Delta z} + \frac{D_+ \cdot (G_i - G_v)}{\Delta r} - H\right]^n_{i,j}$$

$$\left[I + \Delta t\left(\frac{D_+ \cdot A_-}{\Delta z} + \frac{D_- \cdot A_+}{\Delta z}\right) + \Delta t\left(\frac{D_+ \cdot B_-}{\Delta r} + \frac{D_- \cdot B_+}{\Delta r}\right) - \frac{\Delta t}{\delta r}(\bar{\delta} G_v)\right]^n_{i,j} \delta U^{\overline{n+1}}_{i,j} = \Delta U^n_{i,j}$$

$$\Delta U^{\overline{n+1}}_{i,j} = U^n_{i,j} + \delta U^{\overline{n+1}}_{i,j} \tag{5}$$

Corrector

$$\Delta U^{\overline{n+1}}_{i,j} = -\Delta t\left[\frac{D_- \cdot F_i}{\Delta z} + \frac{D_- \cdot (G_i - G_v)}{\Delta r} - H\right]^{\overline{n+1}}_{i,j}$$

$$\left[I+\Delta t\left(\frac{D_+\cdot A_-}{\Delta z}+\frac{D_-\cdot A_+}{\Delta z}\right)\right.$$

$$+\Delta t\left(\frac{D_+\cdot B_-}{\Delta r}+\frac{D_-\cdot B_+}{\Delta r}\right)$$

$$\left.-\frac{\Delta t}{\delta r}(\bar{\delta}G_v)\right]_{i,j}^{\overline{n+1}}\delta U_{i,j}^{n+1}=\Delta U_{i,j}^{\overline{n+1}}+\Delta S_{i,j}^{n}$$

$$\Delta U_{i,j}^{n+1}=\tfrac{1}{2}(U_{i,j}^{n}+U_{i,j}^{\overline{n+1}}+\delta U_{i,j}^{n+1}) \qquad (6)$$

where

(1) superscripts n, $\overline{n+1}$, and $n+1$ refer to the present, predicted and new solution values,

(2) subscripts i and j represent mesh point locations,

(3) ΔU represents the temporal change in the solution during time interval Δt and is evaluated by a local explicit finite difference approximation,

(4) D_+, D_-, and $\bar{\delta}$, represent forward, backward and central difference approximations, respectively,

(5) $\Delta t\left(\frac{\partial U}{\partial t}\right)^{n+1}=\delta U^{n+1}$,

(6) A and B represent the Jacobian matrices, and S represents the similarity transforms used to diagonalize the Jacobians.

An algebraic grid generation scheme is employed, allowing clustering in both the radial and axial directions. This ensures accuracy in the laminar sublayer adjacent to the wall, and improves the convergence by capturing the entrance effects with higher resolution.

Due to specific interest in nuclear thermal rocket propulsion, hydrogen is used as the working fluid. A hydrogen properties package is incorporated into the computer code, allowing the real gas properties to be accurately accounted for. Interpolation techniques are applied to a large data base [3] to obtain specific values as required. The database is composed of two separate parts. The first uses data from the National Bureau of Standards (now National Institute of Standard & Technology) over a temperature range 13.8–3000 K. NASA simulated data makes up the second part, ranging from 3000 to 10 000 K. A simple equilibrium model is used to account for dissociation of hydrogen. This feature is critical for the present calculation since the properties vary substantially in the flow domain.

Three categories of heat transfer boundary conditions are analyzed, an adiabatic surface, a constant or varying temperature surface, and a constant or varying heat flux surface. In this analysis the boundary conditions are not time dependent, but may vary from one axial location to another. Cases involving the heat-flux boundary condition, a Neumann-type boundary condition, proved difficult to solve at acceptable convergence rates. The method used for overcoming this problem will be discussed in the sections which follow. A one-sided differencing scheme

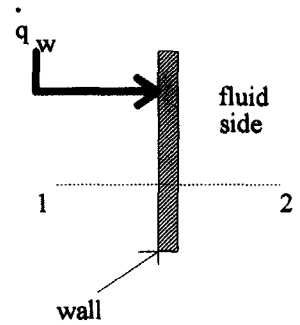

Fig. 1. Heat transfer boundary condition nomenclature.

is used in deriving the boundary conditions shown below. The wall heat flux boundary condition is approximated using the wall-temperature gradient. As shown in Fig. 1, an extrapolation has been used at the solid boundary. The boundary conditions specified in the algorithm are as follows:

$$u_{i,1}=-u_{i,2} \qquad \text{no slip condition} \qquad (7)$$

$$v_{i,1}=-v_{i,2} \qquad \text{radial velocity condition} \qquad (8)$$

$$T_{i,1}=\begin{cases} T_{i,2} & \text{adiabatic condition} \\ 2T_{i,w}-T_{i,2} & \text{specified wall temperature} \\ T_{i,2}+\dfrac{q_w}{k}(r_{i,2}-r_{i,1}) & \text{specified wall heat flux.} \end{cases} \qquad (9)$$

The solution procedure of the governing equations is of the iterative form. The residuals presented in this analysis are of the form shown in equation (10) below.

$$\text{Residual}=\frac{\sum_{i=1}^{i_{max}}\sum_{j=1}^{j_{max}}\sqrt{(U_{i,j}^{n}-U_{i,j}^{n-1})^2}}{(i_{max})(j_{max})} \qquad (10)$$

where $U_{i,j}^{n}$ and $U_{i,j}^{n-1}$ refer to the present and old solution values, respectively.

These residuals show the accuracy of the solution of the momentum and energy equations, as well as the rate of convergence of the governing equations. The residuals approach an asymptotic converged solution which is in the same order with the machine error. The flux imbalance across computational cells is also checked to ensure that convergence has been achieved.

3. TURBULENCE MODELING

The accurate modeling of near-wall turbulence is crucial to obtain accurate predictions for parameters such as heat-transfer coefficients. For high Reynolds number flows in simple geometries (streamlined), with a proper use of constants the algebraic models exhibit good accuracy. However, if this analysis to be expanded to include intermediate or very high Reynolds number flows or flow in complex geometries,

further investigation of turbulence modeling is needed.

The Baldwin–Lomax algebraic turbulence model [4] is used in this analysis. This model has the advantage of avoiding the necessity for finding the edge of the boundary layer. The effects of turbulence are simulated in terms of the eddy viscosity coefficient, μ_t.

Near the wall the Prandtl–Van Driest formulation for turbulent viscosity is used,

$$(\mu_t)_{\text{inner}} = \rho k^2 y^2 \left[1 - \exp\left(\frac{y^+}{A^+}\right)\right]^2 |\omega| \tag{11}$$

where

$$|\omega| = \sqrt{\left(\frac{\partial u}{\partial r} - \frac{\partial v}{\partial z}\right)^2}.$$

In the outer region, away from the wall the eddy viscosity may be written as

$$(\mu_t)_{\text{outer}} = KC_{\text{cp}} F_{\text{wake}} F_{\text{kleb}}(y) \tag{12}$$

$$F_{\text{wake}} = y_{\max} F_{\max} \tag{13}$$

where $F_{\max}$ is the maximum value of $F(y)$ in a radial profile,

$$F(y) = y|\omega|\left[1 - \exp\left(-\frac{y^+}{A^+}\right)\right] \tag{14}$$

and $y_{\max}$ is the value of y at which this occurs, and

$$F_{\text{kleb}}(y) = \left[1 + 5.5\left(\frac{C_{\text{kleb}} y}{y_{\max}}\right)^6\right]^{-1}. \tag{15}$$

The constants are specified as follows:

$$A^+ = 26$$

$$k = 0.4$$

$$K = 0.0168$$

$$C_{\text{cp}} = 1.6$$

$$C_{\text{kleb}} = 0.3.$$

The selection of the inner and outer formulation is important. The minimum value of y (distance measured from the wall), for which the two formulations give the same value, is known as the crossover point. For y values less than the crossover point value the inner equation is used, while for y values greater than the crossover point value the outer formulation is used. In the original Baldwin–Lomax turbulence model an additional equation for the calculation of F_{wake} is presented. However, for the applications in this study where there is no flow separation this wake formulation is not justified.

Visbal and Knight [5] found the constants C_{cp} and C_{kleb} to be dependent upon flow Mach number. For flows over the range $0 \leqslant M_\infty \leqslant 3$ the constants varied by a factor of two. Should the flow be separated they found that errors may occur in the determination of the length scales. Granville [6] also studied the model constants. He formulated an equation for the variation of C_{kleb} with a modified Clauser pressure-gradient parameter, for the variation of C_{cp} with C_{kleb}. A formula for the variation of the Clauser factor, k, with Reynolds number, was also presented. After analyzing these modifications the constants presented above were found to be adequate for the subsonic attached boundary-layer type flow studied here.

4. THE METHOD OF ENTHALPY BALANCING

The application of this method was necessary to obtain solutions at acceptable rates of convergence when using the heat flux boundary conditions. The method applies the fundamental principle that, at steady state, the total heat into a section must equal the total heat out of the section. The enthalpy balance is based upon a velocity and temperature field which are approaching the steady state, and the accuracy of the balance is limited by the accuracy of the developing flow fields compared to these steady-state values. As the solution approaches steady state the accuracy improves. Once the steady-state flow has been achieved, the enthalpy balance no longer has any effect on the computation. The enthalpy balance serves only to accelerate the rate at which steady-state flow is achieved. In this analysis it is assumed that there is no heat generation. There is no reason, however, why this should not be added to the formulation if required.

Applying the principle of an enthalpy balance, as shown in Fig. 2, where Q_1 is the total heat flowing into the section, Q_2 is the total heat added through the wall, and Q_3 represents the total heat leaving the section, the following is true:

$$Q_1 + Q_2 = Q_3. \tag{16}$$

This assumes the kinetic losses to be negligible, which is acceptable for the subsonic flows examined here. For cases in which these losses are not negligible, equation (16) may be simply extended. Expanding equation (16),

$$\bar{M} c_{\text{p}}(T_{3\text{bulk}} - T_{1\text{bulk}}) = 2\pi r l q_{\text{w}}. \tag{17}$$

Assuming the bulk inlet temperature, $T_{1\text{bulk}}$, is known, then the only unknown is $T_{3\text{bulk}}$, the bulk exit temperature. The above equation may be applied over as many individual sections as is required, and may be written in integral form as follows:

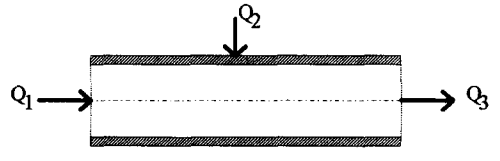

Fig. 2. Diagram showing heat flux nomenclature.

$$\int_{T_{1\text{bulk}}}^{T_{3\text{bulk}}} \bar{M} c_p \, dT = \int_0^l q_w 2\pi r \, dz. \tag{18}$$

Hence,

$$T_{3\text{bulk}}^{HB} = T_{3\text{bulk}} = \frac{2lq_w}{\rho u r \gamma c_v} + T_{1\text{bulk}}. \tag{19}$$

The bulk temperature at the exit of the section may also be found using numerical integration. This intermediate bulk temperature, $T_{3\text{bulk}}^{i}$, may be compared to the bulk temperature computed from the consideration of energy conservation. Since these two temperatures should be equal, they may be used to correct the wall temperature as follows:

$$\varepsilon = \frac{T_{3\text{bulk}}^{HB}}{T_{3\text{bulk}}^{i}}$$

$$\Rightarrow T_w^{new} = \varepsilon T_w^{old}. \tag{20}$$

It was found that, when applying this correction factor, ε, to the flow field, the sudden, sometimes large, change in the wall temperature caused an instability to occur which ultimately led to the code diverging. This follows from the "transient" nature of the solution of the flow fields. If the flow field is insufficiently developed, the temperature corrections at the wall may not be dissipated into the flow quickly enough, resulting in a disproportionately large rise in wall temperature. Should this wall temperature far exceed the fluid temperature, a divergent computation may result. To compensate for this problem a relaxation factor was introduced which allowed the correction to be applied more gradually. This equation may be written as

$$T_w^{new} = T_w^{old} + \omega(\varepsilon - 1) T_w^{old} \tag{21}$$

where ω is the relaxation factor. The empirically evaluated relaxation factors varied from case to case. The larger the wall heat flux the lower the initial relaxation factor, and the lower the Reynolds number the lower the initial relaxation factor. Successively larger relaxation factors were used within each computation until $\omega = 1$, at which point equations (20) and (21) are identical. It appeared that the best approach was to accelerate ω to unity as quickly as possible, in order to obtain the fastest possible rate of convergence without causing the algorithm to diverge. In some instances over-relaxation was used on computations exhibiting a slow rate of convergence, even with enthalpy balancing.

The enthalpy balance could be applied in two ways. Firstly, a total balance could be performed over the entire pipe, resulting in a large correction factor, since the error in the enthalpy balance is accumulated along the length of the pipe. This meant that care had to be taken in selecting the relaxation factors. The second option was to perform independent enthalpy balances over each axial segment, thereby avoiding the accumulated errors of total enthalpy balancing. Since the correction factor is now much smaller, only one or two relaxation factors need to be specified, and in some cases the use of a relaxation factor even became unnecessary. The method of independent enthalpy was preferred as this somewhat eliminated the difficulties in selecting the correct relaxation factors.

5. NUSSELT NUMBER CORRELATIONS

The evaluation of the heat-transfer mechanism was crucial in validating the results obtained using the newly developed enthalpy balancing scheme proposed here. Four Nusselt number correlations were compared with the numerical results, the Petukhov correlation [7], the Gnielinski equation [8], the Notter–Sleicher formulation [9], and the Karman–Boelter–Martinelli correlation [10]. These correlations are presented in Table 1.

The friction factor, f, in the relations presented in Table 1 is given by [11]

$$f = [1.58 \ln(Re) - 3.28]^{-2}. \tag{22}$$

The correlations are presented for constant-property fully developed flows. They may be modified to capture the inlet flow characteristics and also the variable property characteristics. A property correction may be applied to the friction factor [11] as follows:

$$f = f\left(\frac{T_w}{T_b}\right)^{-0.52}. \tag{23}$$

The Nusselt number may be modified in a similar way [12] as follows:

$$Nu = Nu\left(\frac{T_w}{T_b}\right)^n \tag{24}$$

where

$$n = -\left(\log_{10}\frac{T_w}{T_b}\right)^{1/4} + 0.3.$$

Another value which has been used with success is $n = -0.55$.

Entrance effects may be accounted for [11] using

$$Nu = Nu\left[1 + \left(\frac{l}{d}\right)^{-2/3}\right]. \tag{25}$$

Perkins and Worsoe-Schmidt [13] suggested the following correction:

$$Nu = Nu\left[1 + \left(\frac{l}{d}\right)^{-0.7}\left(\frac{T_w}{T_b}\right)^{0.7}\right]. \tag{26}$$

Combining the Nusselt number correlations with the corrections, the numerical results could be evaluated.

6. RESULTS AND DISCUSSION

The enthalpy balancing scheme was employed to accelerate the rate of convergence. Without this

Table 1. Nusselt number correlations

Correlation	Equation	Range of applicability	Error
Petukhov	$Nu = \dfrac{Re\,Pr(f/2)}{1.07+12.7(Pr^{2/3}-1)(f/2)^{1/2}}$	$0^4 < Re < 5\times10^6$ $0.5 < Pr < 2000$ $l/d > 40$	5–6%
Gnielinski	$Nu = \dfrac{(Re-1000)Pr(f/2)}{1+12.7(Pr^{2/3}-1)(f/2)^{1/2}}$	$2300 < Re < 5\times10^6$ $0.5 < Pr < 2000$ $l/d > 40$	±10%
Notter–Sleicher	$Nu = 5+0.016Re^{a}Pr^{b}$ $a = 0.88-0.24/(4+Pr)$ $b = 0.33+0.5e^{-0.6Pr}$	$0^4 < Re < 10^6$ $0.1 < Pr < 10^4$ $l/d > 25$	±10%
Karman–Boelter–Martinelli	$Nu = \dfrac{Re\,Pr\sqrt{f/2}}{0833[5Pr+5\ln(5Pr+1)+2.5\ln(Re\sqrt{f/2}/60)]}$	$0^4 < Re < 10^6$ $0.5 < Pr < 200$ $l/d > 60$	±8%

scheme it was not possible to obtain convergence of the energy equation within a reasonable number of iterations, as illustrated in Fig. 3. The convergence characteristics are shown for a typical high-wall heat-flux case studied in this analysis. A converged solution was obtained within 1200 iterations when employing enthalpy balancing. The "spikes" in the temperature residual were a result of modifying the relaxation factor presented in equation (21). The influence of the wall-temperature correction was more noticeable in the temperature residual, since the correction was directly applied to the solution of the energy equation. The oscillation in the converged solution is typical for a predictor/corrector type scheme as used here, and is on the order of machine error on the SUN system used in the computations. Under precisely the same conditions, with no enthalpy balancing, the rate of convergence was significantly slower. Convergence was achieved within less than half the number of iterations using enthalpy balancing. The effect of the enthalpy balancing scheme on the convergence rate was dependent upon the Reynolds number, Nusselt number and Mach number. The higher the ratio of the heat flux to the flow rate, the more significant the improvement in the convergence rate using enthalpy balancing.

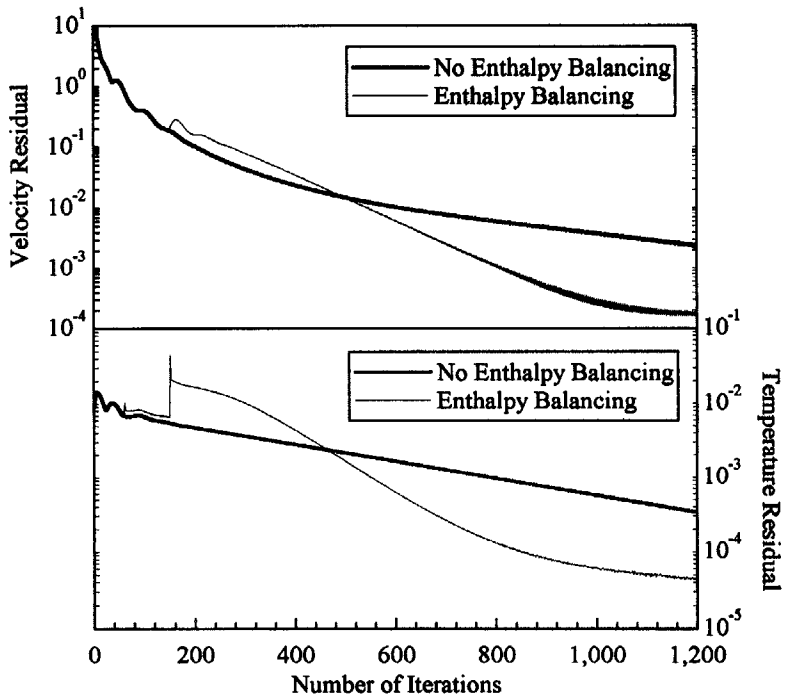

Fig. 3. Comparison of convergence rate with and without enthalpy balancing for uniform wall-heat flux flow.

The slow rate of convergence without enthalpy balancing could be attributed to the inefficiency of the numerically calculated rate of heat transfer via conduction from the wall to the fluid. The enthalpy balancing scheme served to accelerate this heat transfer mechanism, and hence the numerically calculated developing flow-field approached the steady-state solution more rapidly. By applying enthalpy balancing it was possible to obtain solutions for Dirichlet and Neumann thermal boundary conditions within a similar number of iterations.

One of the key purposes of this analysis was to validate the method of enthalpy balancing introduced above. A study of laminar flows provided a good starting point in achieving this goal. Figure 4 illustrates the developing non-dimensional temperature profiles in a laminar pipe flow with a uniform wall-heat flux of 0.1 MW m^{-2}, and an inlet Reynolds number of 1100. The profiles were not fully-developed, but are consistent with those of Presler [14], i.e. the developing temperature profile gradient became steeper with fully-developed centerline values exceeding the Deissler profile [15] for heat input to the system. The Deissler profile refers to the simplified case under which constant properties are assumed for a fully-developed incompressible laminar flow, and the profile shown here is the resulting analytical solution. The fully developed numerical result (FDNUM) with enthalpy balancing and constant fluid properties is also shown in Fig. 4. Since a compressible flow algorithm was used where density is treated as a dependent variable, it could not be made incompressible without significant modification to the code. A very low heat flux was used to obtain the result, causing only a slight axial variation in density. The Deissler profile differs only slightly from this solution which closely approximates the analytical solution. This case study illustrated the successful application of the enthalpy balancing scheme to laminar flows with wall-heat flux-boundary conditions.

The next task was to apply the enthalpy balance to turbulent flows, and to examine the heat-transfer mechanisms of both the isothermal wall and wall-heat flux-boundary conditions. The isothermal wall flow presented here was for an inlet temperature of 1000 K and a constant wall temperature of 1800 K, with an inlet Reynolds number of 6.36×10^4. The wall heat flux flow presented was for a total inlet temperature of 300 K and a constant wall heat flux of 1 MW m^{-2}, with an inlet Reynolds number of 6.18×10^5.

The isothermal wall fully developed turbulent pipe-flow velocity distribution is shown in Fig. 5. The calculated profile was compared to that of the "Law of the Wall" profile correlated by Spalding [16]. The y^+ range selected illustrates the laminar sublayer, the buffer layer, and the turbulent flow regime. The computed result compares within 5% to Spalding's formulation. The experimental data of various investigators exhibits a great deal of dispersion in this regime. With this in mind, the numerical result was found to be satisfactory. The modified Spalding result refers to a modification of Spalding's equation, and contains two additional terms in the equation's expansion. Spalding suggested that the use of additional terms should be investigated, but this argument was not developed.

Figures 6 and 7 illustrate the temperature fields for the isothermal wall and specified wall-heat flux case introduced above. The extreme temperature gradients at the wall in the inlet region of the isothermal wall distribution were clearly visible. These temperature gradients decreased at successive downstream locations. The wall-heat flux temperature field was significantly different. The wall temperature gradient was virtually constant axially. The bulk temperature and wall temperature increased at approximately the same rate once fully developed for the wall heat flux case, while the bulk temperature approached the wall temperature in the isothermal wall case. These characteristics affected the Nusselt numbers.

The calculated Nusselt numbers and selected Nusselt number correlations are compared in Fig. 8 for

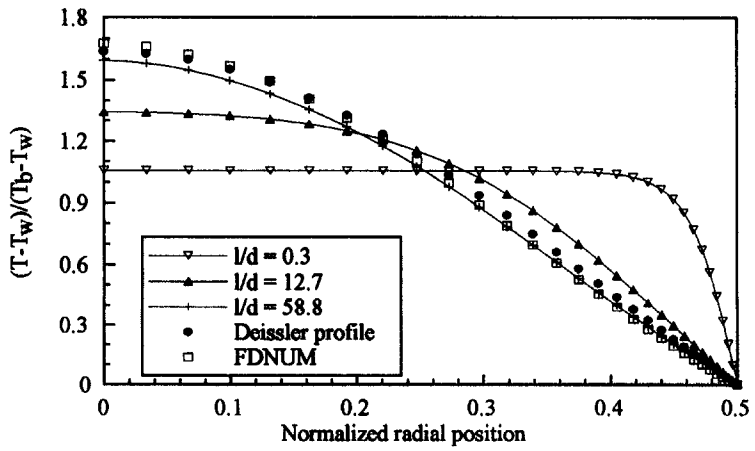

Fig. 4. Non-dimensional radial temperature profiles.

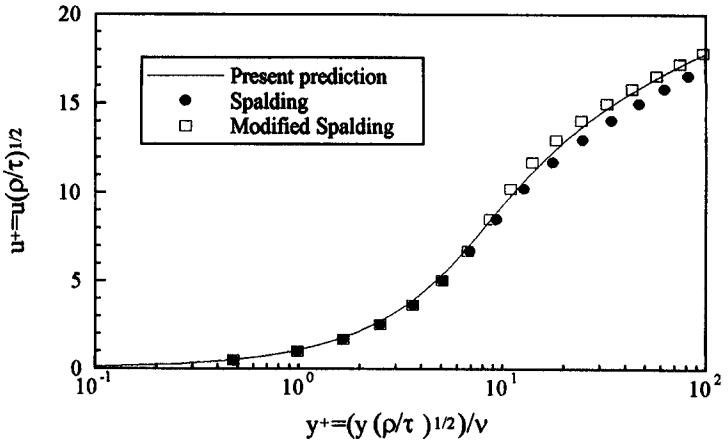

Fig. 5. Fully developed isothermal wall velocity distribution.

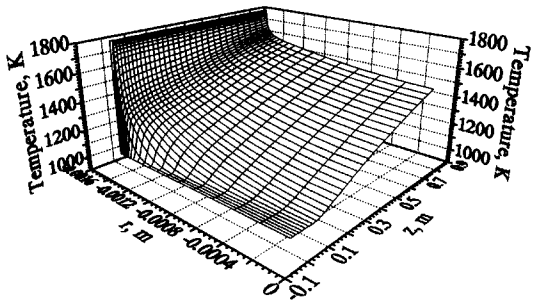

Fig. 6. Temperature distribution for isothermal wall flow.

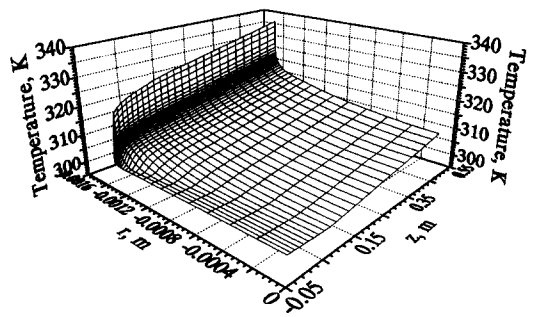

Fig. 7. Temperature distribution for uniform wall-heat flux flow.

the isothermal wall turbulent flow. The four Nusselt number correlations shown in Table 1 were used for comparison with the numerical result. The correlations were corrected for axial distance, as well as for real gas properties. The Petukhov Nusselt number correlation compared closely with the presently computed values, differing by 2% at the exit. The shape of the axial Nusselt number profile may be explained by examining the temperature fields discussed above. The Nusselt number is calculated using the following equation:

$$Nu = \frac{\partial T/\partial y}{(T_w - T_b)} d. \tag{27}$$

As already mentioned the temperature gradient was high at the inlet and so the rapidly decreasing temperature gradient was the dominant term initially, and hence the Nusselt number rapidly decreased. Downstream of the entrance the decreasing denominator became dominant, resulting in the Nusselt number increasing. As the bulk temperature approached the wall temperature the calculated Nusselt number began to flatten out.

The Nusselt numbers shown in Fig. 9 were for a constant wall heat flux of 5 MW m^{-2} and an inlet Reynolds number of 4.6×10^5. For this specified wall-heat flux case, the prediction followed the Petukhov and Gnielinski correlations in the downstream portion of the flow domain, while it followed the Karman–Boelter–Martinelli correlation more closely upstream. The shape of the Nusselt number profile may be explained by examining equation (27) above, relating conduction and convection effects. The temperature gradient at the wall was almost constant since the conductivity varied only slightly with temperature. However, $(T_w - T_b)$, which was initially zero, rapidly increased before approaching a constant value as the flow became fully developed. This explained the continuously decreasing Nusselt number.

The original derivation of the Nusselt number correlations may offer some insight to the disagreement between the correlations themselves, and also the numerical result obtained in this study. All the correlations were formulated assuming constant gas properties, and a fully developed flow. A solution of the equations for heat transfer based on pressure drop result in a dependence of the exponent of the Reynolds number on the Prandtl number. The constants in the theoretical solution could then be adjusted to best fit experimental data. Prandtl was the first to formulate a relationship of this type. The Petukhov correlation represents an improvement on the Prandtl equation, following further analysis of experimental results. The Gnielinski correlation is an extension of the Petukhov correlation, following an extensive survey of exper-

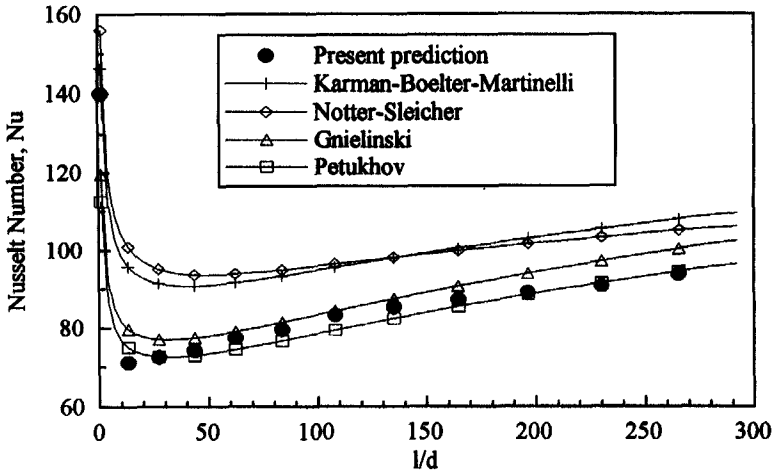

Fig. 8. Nusselt number distributions for isothermal wall flow.

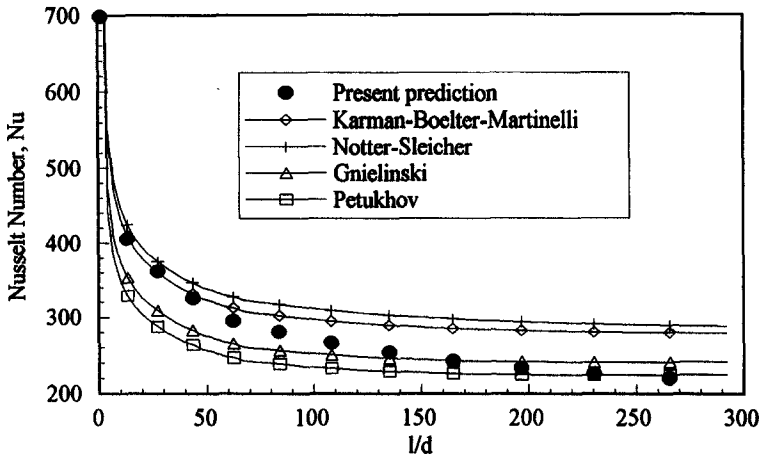

Fig. 9. Nusselt number distributions for wall-heat flux flow.

imental data. Gnielinski modified the Petukhov correlation to be applicable to lower Reynolds number flows as well as the original range specified by Petukhov. This explains the close comparison of the results for the two correlations in this study. The Notter–Sleicher correlation was obtained from a numerical solution of the energy equation using a specified velocity profile and eddy diffusivities, followed by an evaluation of experimental data.

Property and axial distance corrections were applied to all the correlations used. These corrections are derived empirically. The accuracy in the entrance region and sublayer of experimental results is often questionable, especially under extreme conditions. The effects under extreme conditions are often simply extrapolated from less severe regimes. The accuracy of the property correction is also limited to fluids with similar properties to those of the fluids for which the correction was derived. Therefore, added to the error of the base correlations there is the error associated with correcting the correlations for axial distance and variable properties. Bearing these factors in mind it was not surprising that the numerical result obtained in this study did not exactly fit any one correlation, and that the most significant differences were in the entrance region. The temperature and heat flux in the two cases presented in Figs. 8 and 9 were extreme.

The differences between the present prediction and the Nusselt number correlations can be attributed to the substantial variation in fluid properties caused by the high-temperature effects.

7. CONCLUSIONS

A detailed investigation of near-wall heat transfer in laminar and turbulent flow was performed with both Dirichlet and Neumann boundary conditions. The inherent difficulties in obtaining converged solutions with heat-flux boundary conditions were addressed, and an enthalpy balancing scheme was developed. The implementation of the enthalpy balancing scheme allowed fast converging solutions to be obtained. This methodology allowed the convergence

of isothermal wall and wall-heat flux boundary condition cases in a similar number of iterations.

As was expected, the heat transfer was found to be highly dependent upon the Reynolds number, and to a lesser extent on the wall heat flux. The difference in the heat transfer mechanisms between isothermal wall and wall-heat flux-boundary condition flows was explained by analyzing the wall-temperature gradients and the wall to bulk temperature difference. The efficiency of the heat-transfer mechanism was dependent upon the Reynolds number. The Nusselt number increased with increasing Reynolds number, while the magnitude of the wall-heat flux affected the shape of the Nusselt number profile. The flow development was delayed for large wall-heat fluxes.

Near-wall heat transfer in laminar and turbulent flows was analyzed in detail, and a convenient method was formulated for obtaining fast converging numerical solutions of flows with high wall-heat flux boundary conditions.

Acknowledgement—This work was performed for the Department of Defense, Ballistic Missile Defense Organization, Innovative Science and Technology Office, under contract number NAS3-26314, managed by NASA Lewis Research Center.

REFERENCES

1. W. Shyy, *Computational Modeling for Fluid Flow and Interfacial Transport*. Elsevier, Amsterdam (1994).
2. R. W. MacCormack, Current status of numerical solutions of the Navier–Stokes equations, *AIAA 23rd Aerospace Sciences Meeting*, AIAA-85-0032, Reno (1985).
3. J. White, Development of a para and dissociated hydrogen properties package, M.S. Thesis, University of Florida, Gainesville, FL (1993).
4. B. S. Baldwin and H. Lomax, Thin layer approximation and algebraic model for separated turbulent flows, *AIAA 16th Aerospace Sciences Meeting*, AIAA-78-257, Huntsville, AL (1978).
5. M. Visbal and D. Knight, The Baldwin–Lomax turbulence model for two-dimensional shock-wave/boundary-layer interactions, *AIAA J.* **22,** 921–928 (1984).
6. P. S. Granville, Baldwin–Lomax factors for turbulent boundary layers in pressure gradients, *AIAA J.* **25,** 1624–1627 (1987).
7. B. S. Petukhov, Heat transfer and friction in turbulent pipe flow with variable physical properties. In *Advances in Heat Transfer* (Edited by J. P. Hartnett and T. F. Irvine), pp. 503–564. Academic Press, New York (1970).
8. V. Gnielinski, New equations for heat and mass transfer in turbulent pipe and channel flow, *Int. Chem. Engng* **16,** 359–368 (1976).
9. R. H. Notter and C. A. Sleicher, A solution to the turbulent Graetz problem—III. Fully developed and entry region heat transfer rates, *Chem. Engng Sci.* **27,** 2073–2093 (1972).
10. T. Cebeci and P. Bradshaw, *Physical and Computational Aspects of Convective Heat Transfer*, p. 222. Springer, New York (1988).
11. R. K. Shah and R. S. Johnson, Correlations for fully developed turbulent flow through circular and noncircular channels, *Proceedings of the 6th International Heat and Mass Transfer Conference*, Madras, India (1981).
12. W. M. Kays and H. C. Perkins, Forced convection internal flow in ducts. In *Handbook of Heat Transfer Fundamentals* (Edited by W. M. Rohsenow, J. P. Hartnett and E. N. Ganic), Chap. 7. McGraw-Hill, New York (1985).
13. H. C. Perkins and P. Worsoe-Schmidt, Turbulent heat and momentum transfer for gases in a circular tube at wall to bulk temperature ratios to seven. *Int. J. Heat Mass Transfer* **8,** 1011–1031 (1965).
14. A. F. Presler, Analytical and experimental study of compressible laminar-flow heat transfer and pressure drop of a gas in a uniformly heated tube, NASA TN D-6333 (1971).
15. R. G. Deissler, Analytical investigation of fully developed laminar flow in tubes with heat transfer and fluid properties variable along the radius, NACA Technical Note 2410 (1951).
16. D. B. Spalding, A single formula for the "Law of the Wall", *J. Appl. Mech.* **28,** 455–458 (1961).